Supplementary Figures

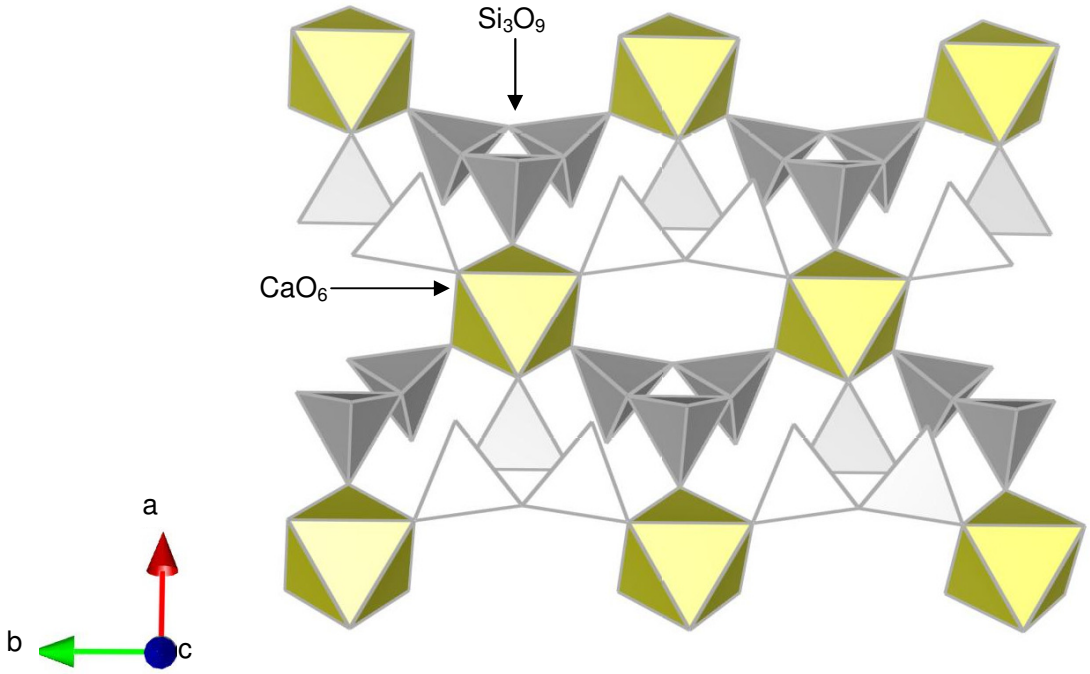

Supplementary Figure S1 | Structure of the [$Ca(SiO_3)_6$] framework.
The gray and white tetrahedra represent SiO_4 complexes, and the yellow octahedra represent $M(1)O_6$ complexes.

(a)

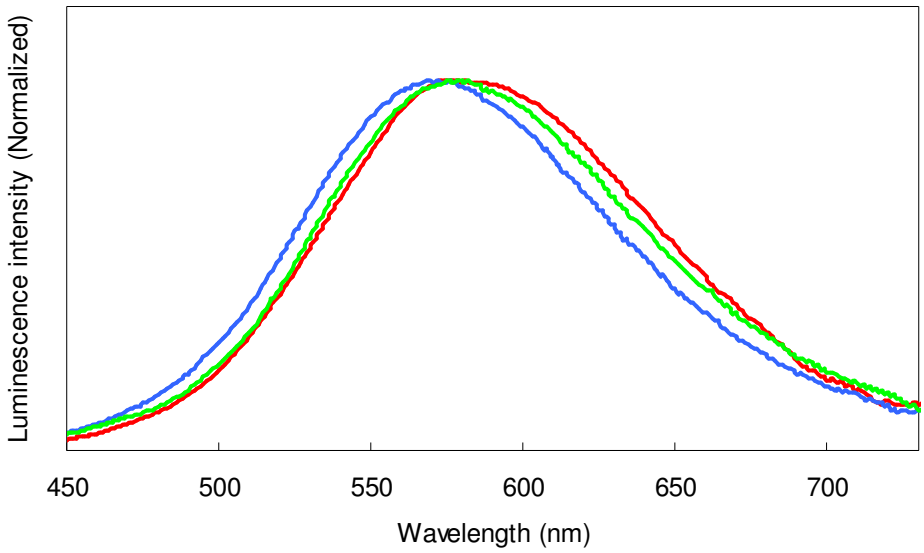

(b)

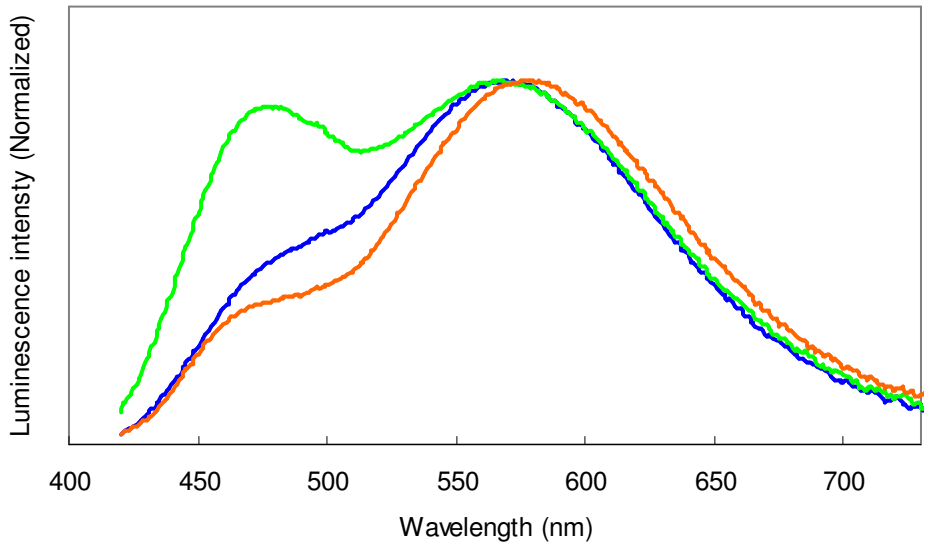

Supplementary Figure S2 | Luminescence spectra of Cl_MS:Eu^{2+}.

The spectra were measured at excitation wavelengths of (**a**) 400 nm and (**b**) 310 nm. The chemical compositions of the phosphors were as follows: $(Ca_{0.34}Sr_{0.62}Eu_{0.04})_7(SiO_3)_6Cl_2$ (λ_D = 574.2 nm, blue curve), $(Ca_{0.40}Sr_{0.56}Eu_{0.04})_7(SiO_3)_6Cl_2$ (λ_D = 575.8 nm, green curve) and $(Ca_{0.58}Sr_{0.38}Eu_{0.04})_7(SiO_3)_6Cl_2$ (λ_D = 577.9 nm, red curve).

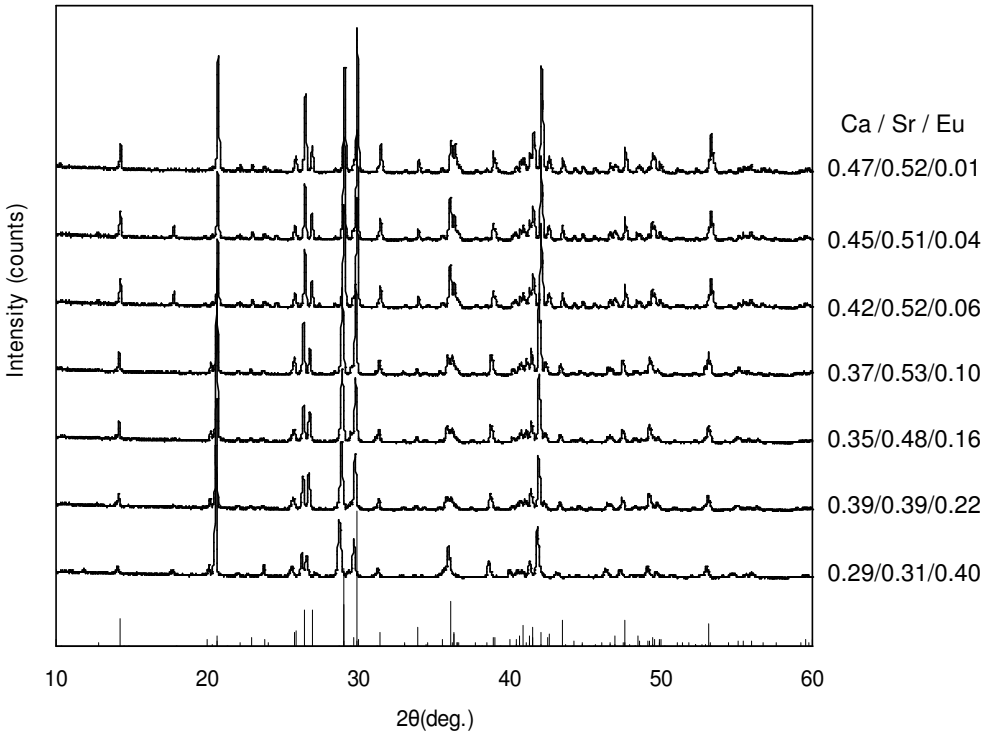

Supplementary Figure S3 | XRD patterns of Cl_MS:Eu^{2+} with various Eu^{2+} concentrations. The right-side values were Ca/Sr/Eu ratios. The pattern of the Cl_MS single crystal was provided at the bottom. The X-ray diffraction patterns of all samples were congruous with the pattern of the Cl_MS single crystal. These samples consisted almost completely of a single phase; only a few impurity peaks were observed.

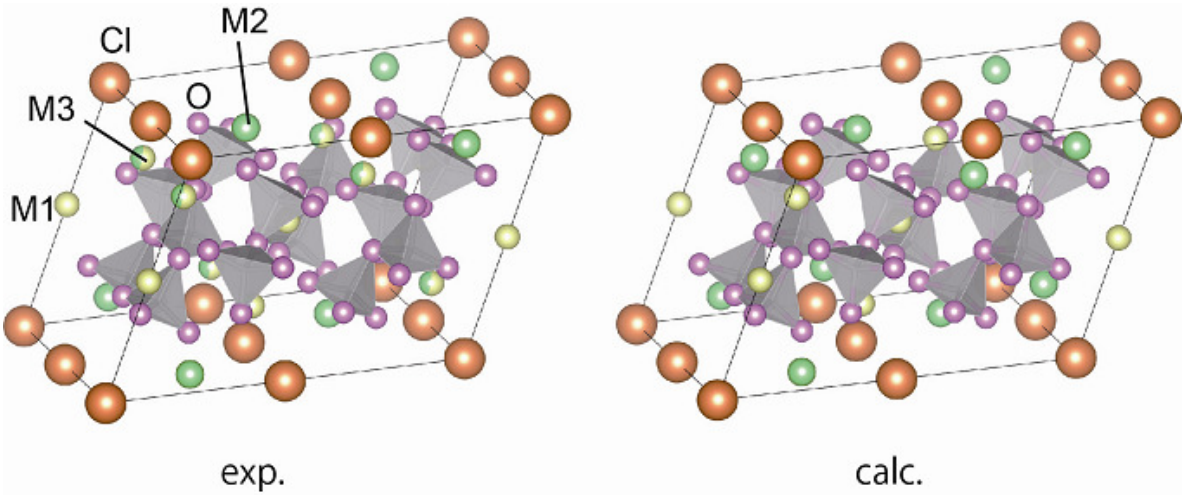

Exp.: a = 13.2925 Å, b = 8.33060 Å, c = 9.17510 Å, α = 90.0°, β = 110.2740°, γ = 90.0°
Calc.: a = 13.2626Å, b = 8.26260Å, c = 9.11170Å, α = 89.5587, β = 110.1988°, γ = 91.0852°

Supplementary Figure S4 | Experimental and calculated structures of Cl_MS:Eu^{2+}. Schematic illustration of the structure of $CaSr_2(Ca_{0.55}Sr_{0.45})_4Si_6O_{18}Cl_2$ at 100 K as determined by single-crystal X-ray diffraction (exp) and the relaxed structure calculated by the projected augmented plane-wave method (calc).

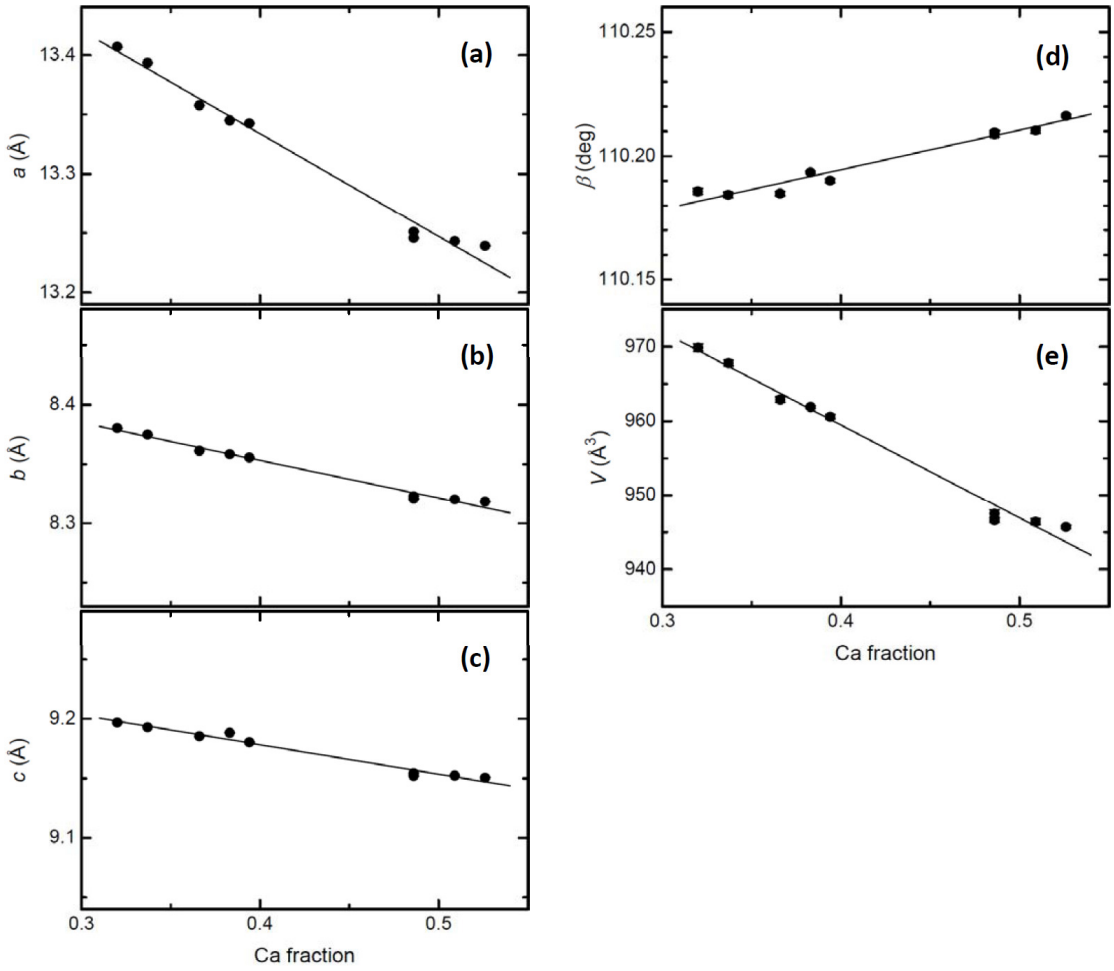

Supplementary Figure S5 | Lattice constants of Cl_MS:Eu^{2+} as a function of Ca fraction.
Lattice constants *a*, *b*, *c*, β and unit cell volume *V* are plotted in **a**, **b**, **c**, **d** and **e**, respectively. Lattice contraction with increasing Ca fraction was greater along the *a*-axis than along the *b*- and *c*-axes.

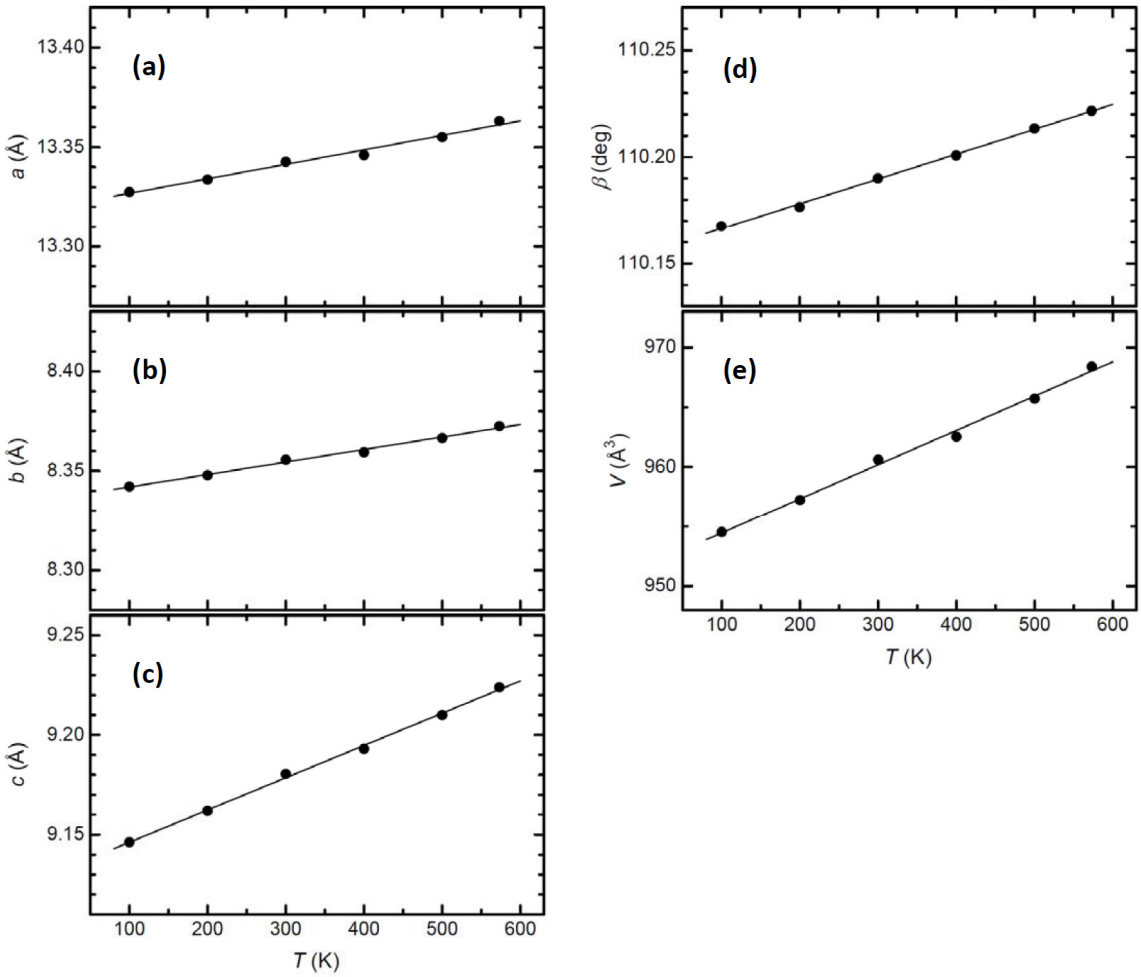

Supplementary Figure S6 | Lattice constants of Cl_MS:Eu^{2+} as a function of temperature. The chemical composition of Cl_MS:Eu^{2+} was $(Ca_{0.40}Sr_{0.56}Eu_{0.04})_7(SiO_3)_6Cl_2$. Lattice constants *a*, *b*, *c*, β and unit cell volume *V* are plotted in **a**, **b**, **c**, **d** and **e**, respectively. The linear thermal expansion coefficients along the *a*-, *b*- and *c*-axes at 300 K were 5.4×10^{-6}, 7.5×10^{-6} and 1.8×10^{-5}, respectively.

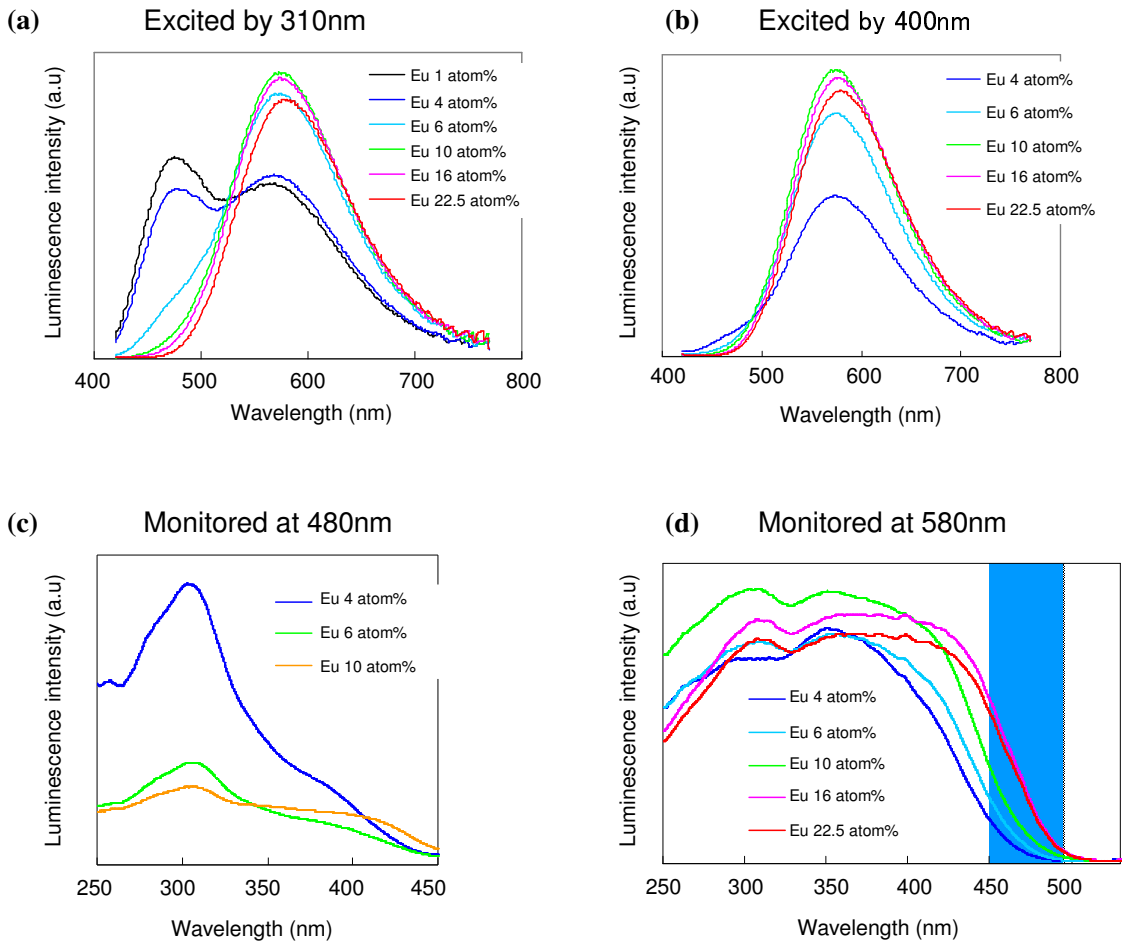

Supplementary Figure S7 | Concentration quenching of Cl_MS:Eu^{2+}.

(**a, b**) Luminescence spectra of Cl_MS:Eu^{2+} species with various Eu^{2+} concentrations upon excitation at 310 and 400 nm, respectively. (**c, d**) Excitation spectra of Cl_MS:Eu^{2+} species with various Eu^{2+} concentrations monitored at 480 and 580 nm, respectively. The area hatched in blue in **d** indicates the wavelength of blue light. When the Eu^{2+} concentration exceeded 4 atom%, the 480-nm band was drastically affected by concentration quenching in **a** and **c**. The main emission band (580 nm) of Cl_MS:Eu^{2+} exhibited no concentration quenching in **b**. In **d**, as the Eu^{2+} concentration was increased, the band extended toward the long-wavelength side with no decrease in intensity. However, in the sample with the highest intensity (10 atom% Eu), the absorption in the blue region was weak.

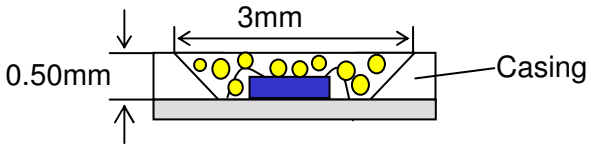

Supplementary Figure S8 | Schematic of surface-mount device (SMD) pc-LED.

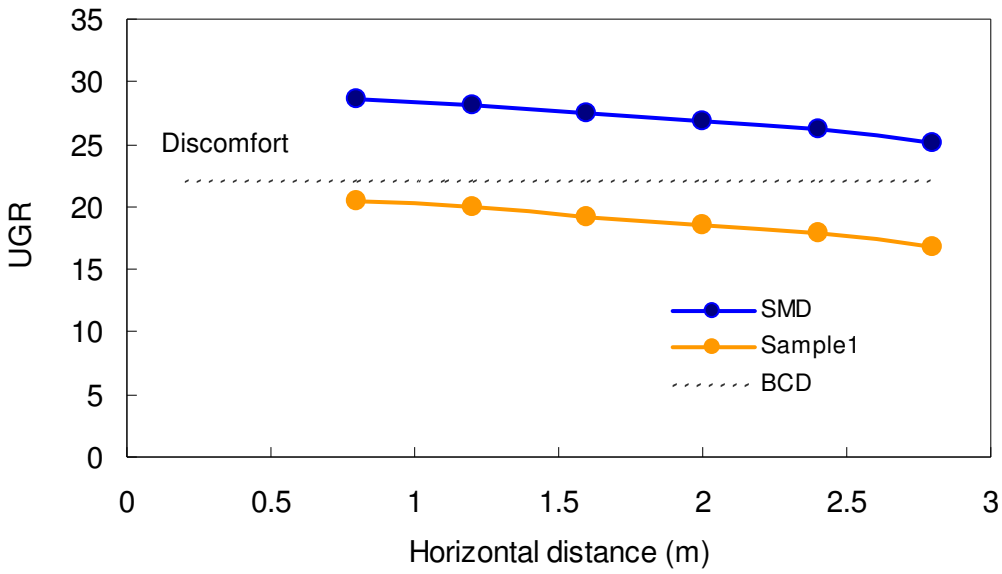

Supplementary Figure S9 | Unified glare ratings (UGRs) of sample 1 and SMD pc-LEDs as a faunction of horizonatal distance T.

The dotted line indicates the borderline between comfort and discomfort (BCD). The UGR of sample 1 was below the BCD at all horizontal distances.

Supplementary Tables

	$(Ca_{0.46}Sr_{0.54})_7(SiO_3)_6Cl_2$	
Data collection		
Temperature	100 K	300 K
Space group	*C*2/*m*	*C*2/*m*
Cell dimensions		
a (Å)	13.2688(3)	13.2925(4)
b (Å)	8.3249(2)	8.3306(2)
c (Å)	9.1323(3)	9.1751(2)
α, β, γ (°)	90, 110.234(2), 90	90, 110.274(2), 90
Resolution (Å)	0.60	0.60
R_{merge}	0.0281	0.0159
$I/\delta I$	> 0	> 0
Completeness (%)	0.966	0.999
Redundancy	4.25	5.23
Refinement		
Resolution (Å)	0.60	0.60
No. reflections	2335	2422
*R*1	0.0249 ($I/\delta I > 2$)	0.0207 ($I/\delta I > 2$)
No. atoms	14	14

Supplementary Table S1 | X-ray crystal structure determination of undoped single-crystal Cl_MS.

T (K)	a, b, c, β, V	R_{WP}, R_I
100	13.3276(2), 8.3421(1), 9.1462(1), 110.168(1), 954.5(4)	0.0574, 0.0460
200	13.3338(2), 8.3479(1), 9.1619(1), 110.177(1), 957.2(4)	0.0605, 0.0485
300	13.3427(1), 8.3557(1), 9.1805(1), 110.190(1), 960.6(3)	0.0577, 0.0451
400	13.3461(2), 8.3594(1), 9.1930(1), 110.201(1), 962.5(4)	0.0602, 0.0511
500	13.3551(2), 8.3666(1), 9.2100(1), 110.213(1), 965.7(4)	0.0635, 0.0544
573	13.3632(2), 8.3725(1), 9.2239(1), 110.222(1), 968.4(4)	0.0627, 0.0502

Supplementary Table S2 | Temperature dependence of the Rietveld refinements of Cl_MS:Eu^{2+} powder.

The temperature dependence of the crystal structure of Cl_MS:Eu^{2+} was investigated at 100, 200, 300, 400, 500 and 573 K with a powder sample with a chemical composition of $(Ca_{0.40}Sr_{0.56}Eu_{0.04})_7(SiO_3)_6Cl_2$. The lattice constants and the reliability factors of Cl_MS:Eu^{2+} were determined from the Rietveld refinements. No phase transitions were observed from 100 to 573 K.

Chemical composition	Emission colour	Internal quantum efficiency	Absorption
$(Ca_{0.45}Sr_{0.51}Eu_{0.04})_7(SiO_3)_6Cl_2$	Yellow	0.98	0.49
$(Ca_{0.42}Sr_{0.52}Eu_{0.06})_7(SiO_3)_6Cl_2$	Yellow	0.97	0.74
$(Ca_{0.37}Sr_{0.53}Eu_{0.10})_7(SiO_3)_6Cl_2$	Yellow	0.94	0.90
$(Ca_{0.35}Sr_{0.49}Eu_{0.16})_7(SiO_3)_6Cl_2$	Yellow	0.88	0.94
$(Ca_{0.39}Sr_{0.39}Eu_{0.22})_7(SiO_3)_6Cl_2$	Yellow	0.84	0.95
$(Ca_{0.29}Sr_{0.31}Eu_{0.40})_7(SiO_3)_6Cl_2$	Yellow	0.49	0.94
$(Ca,Sr,Eu)_5(PO_4)_3Cl$	Blue	0.99	0.91
$(Ba,Eu)MgAl_5O_{17}$	Blue	0.97	0.69
$(Sr,Eu)Ga_2S_4$	Green	0.90	0.83
$(Ba,Sr,Eu)_2SiO_4$	Yellow	0.90	0.92
(Ca,Eu)S	Red	0.72	0.70
$(Sr,Ca,Eu)AlSiN_3$	Red	0.94	0.74

Supplementary Table S3 | Internal quantum efficiency (IQE) and absorption of Cl_MS:Eu^{2+} and other phosphors.

Even though the Eu^{2+} fraction in Cl_MS:Eu^{2+} increased more than 20 atom%, the IQEs of Cl_MS:Eu^{2+} declined only slightly.

pc-LED	Luminous flux (lm)	Colour rendering index (Ra)	Colour temperature (K)
Sample 1	88	82	4,100
Sample 2	79	71	4,900
Sample 3	60	87	3,900

Supplementary Table S4 | Performance of the fabricated pc-LEDs.

Sample 1 ,violet chip coupled with $(Ca_{0.37}Sr_{0.53}Eu_{0.10})_7(SiO_3)_6Cl_2$ and the blue phosphor APT:Eu^{2+}. Sample 2, blue chip coupled with YAG:Ce^{3+}**.** Sample 3, violet chip coupled with mixture of APT:Eu^{2+} ,β-SiAlON:Eu^{2+} and S-CASN:Eu^{2+}. The performance of the samples was observed at an operation current of 350 mA.

Supplementary Methods

Crystal structure determination. Single-crystal synchrotron radiation X-ray diffraction (SR-XRD) experiments on an undoped $(Ca_{0.46}Sr_{0.54})_7(SiO_3)_6Cl_2$ (Cl_MS) crystal were carried out with the large cylindrical imaging plate camera[42] at SPring-8 beamline BL02B1 (Hyogo, Japan). The crystal ($50 \times 40 \times 10$ μ m^3) was mounted on a glass rod. The wavelength of the incident X-rays was ca. 0.35 Å. The sample temperature was controlled at 100 or 300 K by means of a low-temperature N_2 gas flow system. The initial atomic positions were determined by a direct method using SIR2004[43]. The structure model was refined by full-matrix least-squares methods with anisotropic displacement parameters using SHELXL-97[44].

Powder SR-XRD experiments for nine Eu^{2+}-doped Cl_MS powder samples were carried out with the large Debye–Scherrer camera[45] at SPring-8 beamline BL02B2. The wavelength of the incident X-rays was ca. 0.80 Å. Diffraction patterns of Cl_MS:Eu^{2+} samples sealed in glass capillaries were recorded on the imaging plate. Sample temperatures were controlled by means of a N_2 gas flow system. Structure refinements based on the undoped Cl_MS structure were carried out by means of the Rietveld method using SP[46] with a resolution of $d > 0.66$ Å.

Concentration quenching of Cl_MS:Eu^{2+}. Samples for concentration quenching studies were prepared by the self-flux method. The phase purity of the resulting powders was checked by X-ray powder diffraction with a Rigaku RINT-Ultima III diffractometer with Cu Kα radiation at 40 kV and 40 mA. The chemical composition was determined by X-ray fluorescence analysis (Rigaku RIX1000). The optical measurements of these samples are described in the Methods section of the main text.

Comparison of pc-LEDs with a surface-mount device (SMD) pc-LED. We calculated the unified glare ratings (UGRs) of the sample 1 pc-LED and a SMD pc-LED by means of the following equation:

$$\mathrm{UGR} = 8 \log[(0.25/L_b) \cdot \Sigma(L^2\omega/p^2)] \quad \text{(S1)}$$

where L_b is the background luminance (cd/m^2), L is the source luminance (cd/m^2), ω is the solid angle of the source (sr), and p is the position index (describing the positional relationship between the light source and the line of sight)[47]. We assumed an indoor environment and chose 50 cd/m^2 for the background luminance. The values of the luminance were adopted as the source luminance, when the sample 1 and the SMD pc-LEDs were operated at 350 mA. The position index p was determined from the location of an observer and the light source. The location of the light source was indicated by three distance elements: a parallel direction R, a vertical direction H and a horizontal direction T to the fixation axis of an observation. This calculation was performed with R =

1 m, H = 2 m and T = 0.8–2.8 m.

Supplementary References

42. Sugimoto, K et al. Extremely high resolution single crystal diffractometory for orbital resolution using high energy synchrotron radiation at SPring‐8. *AIP Conf. Proc.* **1234**, 887 (2010).

43. Burla, M.C. *et al.* SIR2004: an improved tool for crystal structure determination and refinement. *J Appl. Cryst.* **38**, 381 (2005).

44. Sheldrick, G. M. A short history of SHELX. *Acta Cryst. A* **64**, 112 (2008).

45. Nishibori, E *et al*. The large Debye–Scherrer camera installed at SPring-8 BL02B2 for charge density studies. *Nucl. Instrum. Meth. A* **467-468,** 1045 (2001).

46. Nishibori, E *et al*. Accurate structure factors and experimental charge densities from synchrotron X-ray powder diffraction data at SPring-8. *Acta Cryst. A* **63,** 43 (2007).

47. Guth, S. K. A method for the evaluation of discomfort glare. *Illum. Eng.* **58**, 351-364 (1963).